Olin College of Engineering

Corrosive Failure of a VW Jetta Wolfsburg RXII Rim

Kat Brookshier, Erica Chin, Rachel Fox

Failure Analysis and Prevention
11/19/2010

Corrosive Failure of a VW Jetta Wolfsburg RXII Rim

Kat Brookshier, Erica Chin, Rachel Fox

Abstract

The rims of two BBS RXII wheels from a 2001 Volkswagen Jetta Wolfsburg edition were examined to determine the role of corrosion in the failure of the wheels. It was determined that corrosion of the rims allowed air to escape through the corroded areas, which led to rapid loss of tire pressure, causing the wheels to fail. Three types of corrosion were observed on the rims. A region of crevice corrosion was found where the tire formed a seal with the rim, intergranular corrosion was observed at the microstructural level, and filiform corrosion was observed under the polymer coating which covered the rims. It was concluded that the owners of these rims were not at fault for the failure, and that Volkswagen should have been held accountable for replacing the failed rims.

1. Introduction

Rapidly deflating tires pose a safety hazard to drivers and an inconvenience to car owners who must constantly re-inflate the tires to maintain the manufacturer recommended level of air pressure. In summer 2008, rapid tire deflation occurred in a set of BBS wheels on a 2001 Volkswagen Jetta Wolfsburg edition.

The car owner was displeased to discover that the cast aluminum wheel rims were corroding within months after the purchase of the car. The car was driven in Massachusetts between 2001 and 2008. The rims were cleaned about once a month during the usage period. Because New England has snowy road conditions, the rims were subject to road salt and moisture, conditions that make aluminum alloys high susceptible to corrosion.

By 2008, the tires were deflating so quickly that they had to be refilled every two days [3]. It was postulated that there might have been a link between the corrosion on the rims and tire deflation.

The car owner reported observing a corrosive pattern that formed at the outer lip of the rim, appearing much like growing interconnected filaments of frost. Additionally, the corrosion occurred beneath the clear lacquer on the rims, at the metal-lacquer interface. Many other owners posted pictures of rims with similar corrosive behavior on forums [4-5].

The rims investigated in this study displayed several different types of failure, including loss of function, loss of service life, and aesthetic failure. The dangerous combination of these factors forces drivers to make the expensive decision between replacing their tires and staying safe on the road.

1.1. Anatomy

The terms used to describe the wheel-tire assembly is shown in Figure 1. The rubber portion of the assembly is referred to as the tire. The wheel, or the metal part, has two components: a cylindrical shell- referred to as the rim, and a central section with a branching design [6]. In general, the tire provides traction and shock absorption, while the rim provides structure for the wheel [7]. Optimized air pressure between the rim and the tire allows for the best wheel performance on the road. For sufficient inflation of the tire, air must be enclosed in the space between the tire and the rim. The successful enclosure and preservation of air pressure depends on the seal formed between the surfaces of the rim and tire. More specifically, the beads (Figure 1) of the tire must fit tightly to the raised plateaued region of the rim, known as the bead seat area.

Figure 1: Anatomy of a wheel-tire assembly. The tire is marked solid black. The cylindrical portion of the wheel, the rim, is marked in grey. Air is enclosed between the tire and rim; air pressure within the chamber is maintained by the seal formed between the tire bead and the bead seat. Image modified from [1-2].

2. Methods

2.1. Visual Examination

Visual examination of the rim was conducted by removing the tire so all surfaces could be examined.

The variation of corrosion product concentration levels relative to corrosion product location on the rim was noted macroscopically. For ease of examination, a cross-sectional cut of the rim was made, as shown in Figure 2. Regions with greater presence of corrosion product were cut, as shown in Figure 3, for visual analysis on the cross-sectional surfaces at the microscopic level.

Figure 2: Cross-sectional cuts.

2.2. Pressure Testing

To quantify air loss, a wheel specimen was taken to a gas station and filled with air. Data for tire air pressure was taken over the course of two hours using a hand-held tire pressure gauge.

2.3 X-Ray Diffraction

A Shimadzu XRD-7000 MAXima x-ray diffractometer was used to determine the major crystalline phases of the rim alloy. For the XRD analysis, one millimeter thick sections of the rim alloy were prepared using a Buehler ISOMET 500 precision saw.

X-ray diffraction was also performed on the corrosion product found on the surface of the rims. The corrosion product was gathered by scraping the corroded surface of the rim with a razor blade.

Jade, a powder diffraction analysis package from Materials Data, Inc. was used to analyze the XRD results. Peak identification was performed using automated search/match methods.

2.4 Electron Dispersive X-Ray Spectroscopy (EDS)

A sample was prepared for electron dispersive X-ray spectroscopy (EDS) testing by sectioning, hot mounting in Bakelite, grinding with graduated SiC papers, and polishing to 0.05 micron alumina.

EDS was performed using the JEOL JSM-6060 LV scanning electron microscope and the Thermo Noran System Six energy dispersive X-ray spectrometer. Point and shoot scans, line scans, and bulk scans were used to determine the composition of primary phases in the sample.

EDS of the corrosion product was also performed.

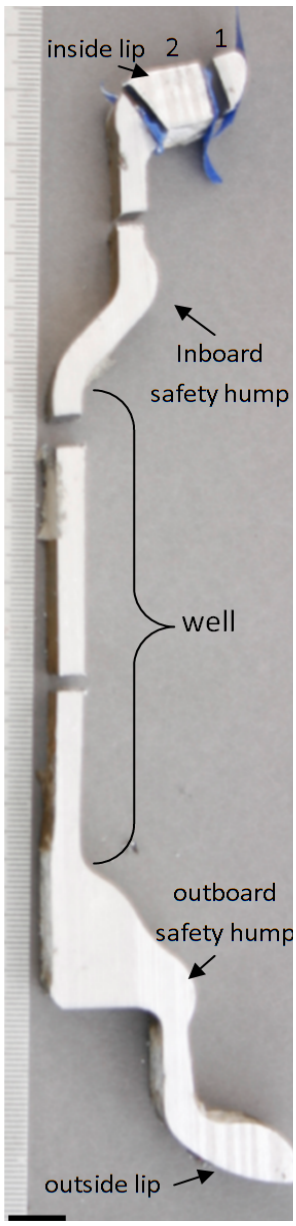

Figure 3: Terms used to reference parts of a rim. Scale bar = 1 cm. Labels 1 and 2 refer to samples used for cross-section surface examination.

2.5 Optical Microscopy

Optical microscopy was performed to observe the microstructure of the alloy. A cross-sectional sample was prepared using the same method outlined for EDS analysis.

Another sample taken from an area of the rim that displayed a large amount of corrosion product on the surface was also observed.

2.6 Scanning Electron Microscopy

Scanning electron microscopy (SEM) was performed to further quantify the observed microstructure of the rim alloy. The sample used for optical microscopy was used for scanning electron microscopy.

SEM was also used to analyze the corrosion product on the surface of the rim, and the microstructure of the corroded alloy.

2.7 Protective Film

Fourier Transform Infrared spectroscopy (FTIR) was used to characterize the peeling coating on the rim. The surfaces of the polymer sample, an example of which is shown in Figure 4, were cleaned with methanol. FTIR spectra were collected with the aid of the software OPUS and were cross-referenced with spectra from the database KnowItAll® AnyWare™.

Figure 4: Flake of plastic coating from outer lip of rim.

3 Results

3.1 Visual Examination

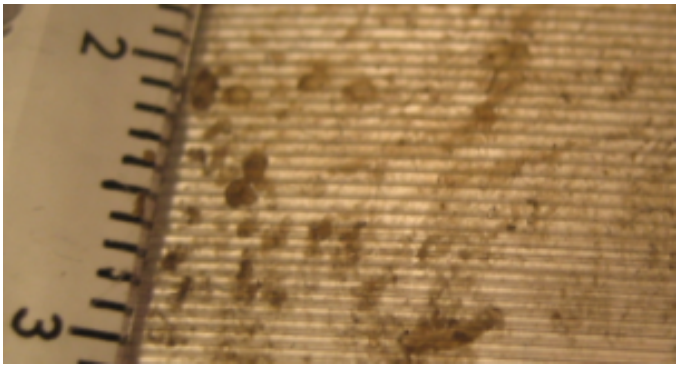

Figure 5: Flake of plastic coating from outer lip of rim.

Preliminary visual inspection of the rim after tire removal revealed peeling plastic coating and extensive white corrosion product concentrated between the edges of the rim and the safety humps, as shown in Figure 3. There was also a noticeable lack of corrosion products and surface ridges at the rim flange area. If not obscured by corrosion products, the surface of the rest of the rim displayed regular ridges, as shown in Figure 5.

3.2 Pressure Testing

The tire pressure test confirmed rapid loss of pressure over time. The tire pressure dropped from 35 psi (a standard air pressure for the tire) to 10 psi in the span of two hours, as seen in **Error! Reference source not found.**6.

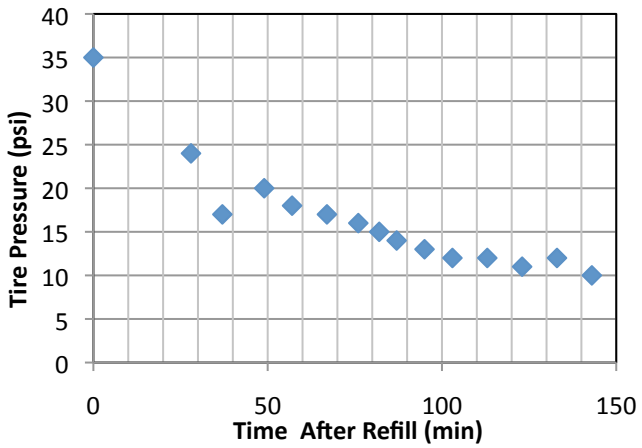

Figure 6: Graph showing air pressure loss from tire over the course of two and a half hours.

Once tire pressure loss was confirmed, the location of the air leak was sought. A mixture of dish soap and water was poured over the tire specimen; the location of growing bubbles indicated the location of air leaks.

Video footage[1] shows that the air leaks were concentrated on the brake side of the wheel. Even when the tire was almost fully deflated, a substantial amount of air was expelled.

3.3 X-Ray Diffraction

XRD showed that the rim was made from an aluminum–silicon alloy, with a composition of 84.8 weight percent aluminum, 8 weight percent silicon, and 7.2 weight percent of an unidentified element. Composition was determined using Jade's Search/Match function as depicted in Figure 7, which identified large aluminum peaks, smaller silicon peaks, and indicated the presence of some other compound with low intensity peaks that were not of adequate intensity for automated search/match analysis.

XRD of the corrosion product resulted in a spectrum containing too much noise for Search/Match analysis. Manual searching/matching based on powder diffraction data from common aluminum corrosion products, however, showed a good match between the corrosion product XRD peaks and those of aluminum trihydroxide ($Al(OH)_3$). Aluminum trihydroxide is the most common corrosion product for aluminum alloys.

3.4 Electron Dispersive X-Ray Spectroscopy

Bulk EDS was performed to determine the rim alloy's composition. Bulk spectroscopy measurements revealed an average composition of 84.61 weight percent aluminum and 12.60 weight percent silicon.

An internal fluorescence peak from silicon may account for the higher silicon weight percent found by the EDS, as compared to the XRD.

Comparison of experimental composition from XRD with literature values supported identification of the alloy as cast aluminum-silicon. The alloy is probably a 4xx.0 cast series, which contains only aluminum and silicon [8-9].

3.5 Optical Microscopy

To confirm the hypothesis of a cast alloy, the microstructure of the metal was examined (Figure 8).

The dendritic structure and casting voids are definitive proof of a cast alloy as opposed to a wrought alloy.

The microstructure is hypoeutectic, which is consistent with a composition between 1.6 and 12.6 weight percent silicon

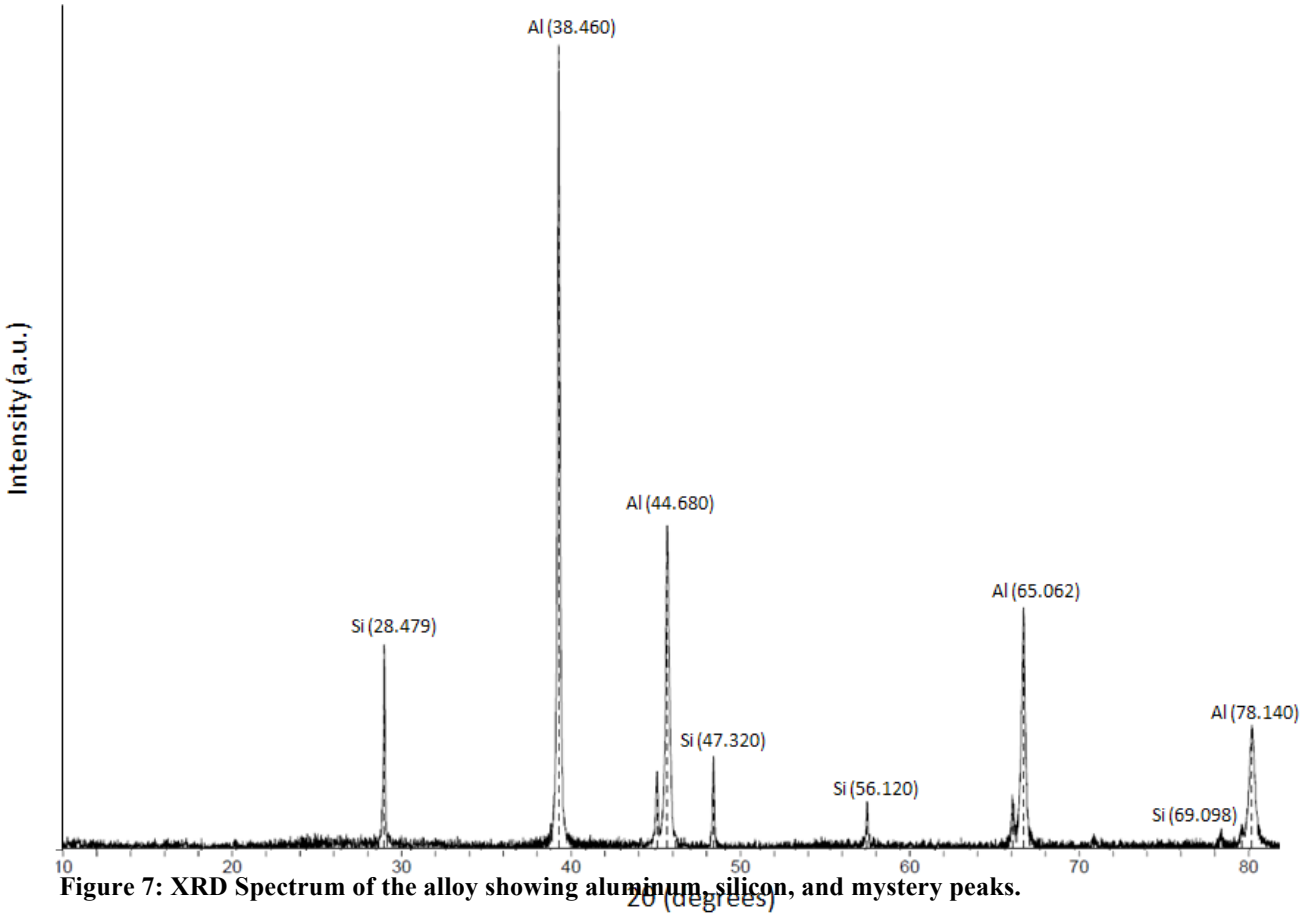

Figure 7: XRD Spectrum of the alloy showing aluminum, silicon, and mystery peaks.

(Figure 9).

Based on visual examination, the alloy is approximately 55% aluminum solid solution dendrites and 45% eutectic solid. These percentages would result in an alloy with 6.55 weight percent silicon, which is closer to XRD estimates (see Appendix for calculations).

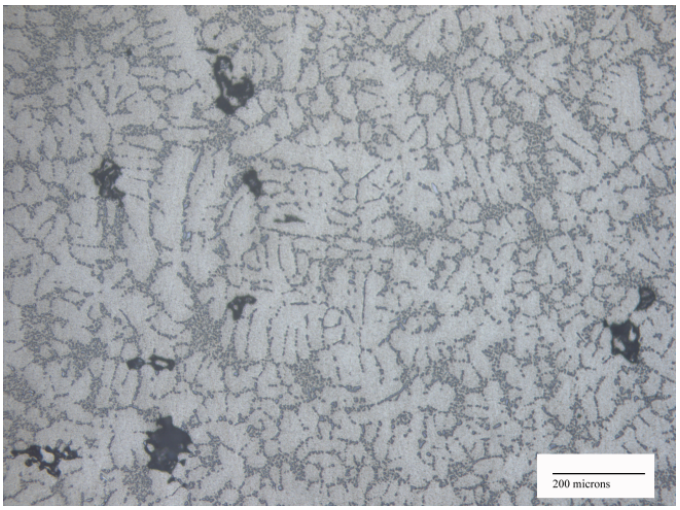

Figure 8: Optical micrograph of a cross-sectional sample of the rim. The dendritic structure (light, aluminum solid solution) and eutectic solid regions (dark, speckled regions) indicate that the rim is a cast, hypoeutectoid Al-Si alloy. Dark areas are casting voids.

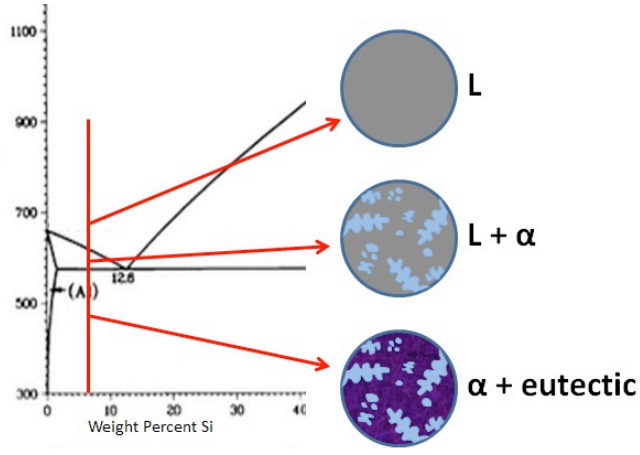

Figure 9: The aluminum-silicon phase diagram and the formation of a hypoeutectic alloy. As the alloy cools, it passes through an α+L phase during which aluminum dendrites nucleate, and then passes over the eutectic line, resulting in a two phase eutectic matrix surrounding the dendrites.

Optical microscopic analysis of a corroded sample revealed selective corrosion of the eutectic solid, or interdendritic, regions of the microstructure (Figure 10).

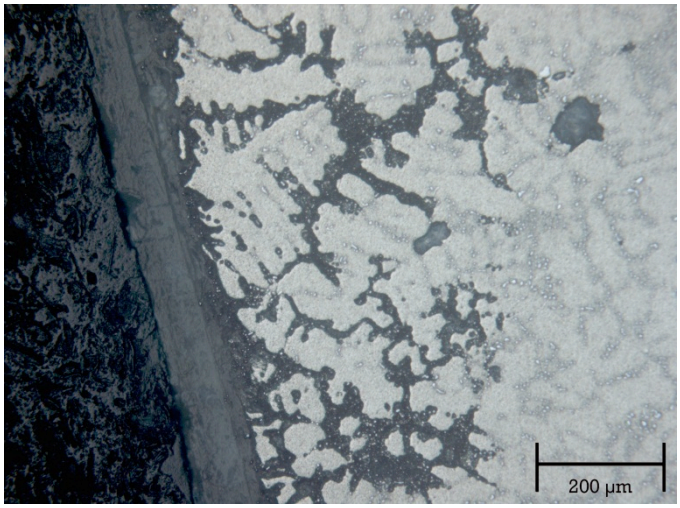

Figure 10: Optical micrograph of a cross-sectional sample from the edge of the corroded rim, showing intergranular corrosion in interdendritic regions.

3.6 Scanning Electron Microscopy

Scanning electron microscopy more clearly showed the two-phase α + β eutectic solid solution between the dendrites. The alpha phase is aluminum which contains approximately 1.6 weight percent silicon in solid solution. The beta phase is silicon which contains approximately 0.1 weight percent in solid solution.

The microscopy, Figure 11, also revealed the presence of silicon solid solution needles which are a result of solidification at the eutectic point (12.6 weight percent Si). These could be a result of non-equilibrium cooling or unequal silicon distribution.

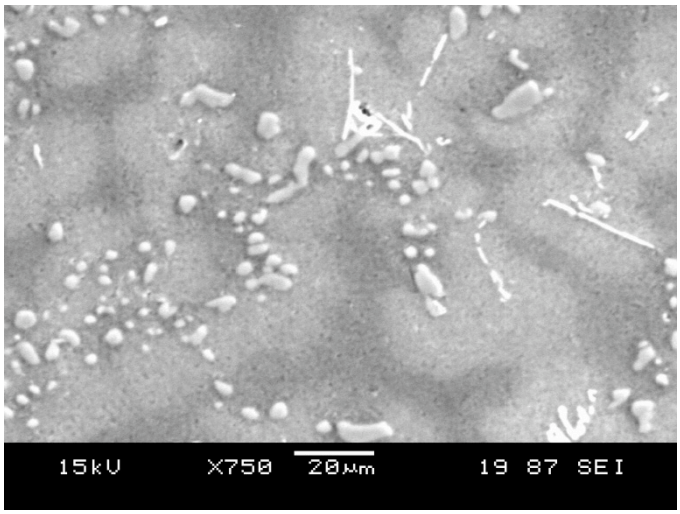

Figure 11: Scanning electron micrograph of the cast rim alloy, showing aluminum solid solution dendrites (dark) with two-phase eutectic solid between dendrites. Light areas are the silicon solid solution phase.

SEM analysis also showed that the corrosive solution had preferentially attacked the boundaries between the silicon and aluminum phases in the eutectic solid region of the alloy, as seen in Figure 12. The presence of some corrosion product on the surface of the metal was observed.

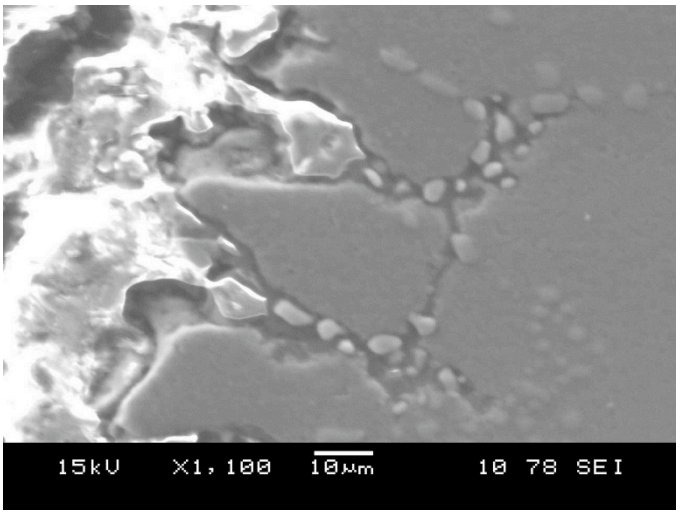

Figure 12: SEM micrograph of the corroded edge of the rim, showing that corrosion attacks aluminum eutectic phase, but not silicon. Corrosion product can be seen on the left (light areas).

3.7 The Protective Film

FTIR spectra of the removed film had the characteristic peaks of acrylic resins [10]. As lacquers, acrylics form coatings through the evaporation of solvents [10]. The sample was closely matched with Macrynal SM 510, as shown in Figure 13. Macrynal SM 510 is a resin used for clear top coats in automotive refinish coatings. Made by Cytec, this liquid resin is designed for weather durability and is advertised to meet the lowest volatile organic compound (VOC) requirement 420 g/l [11].

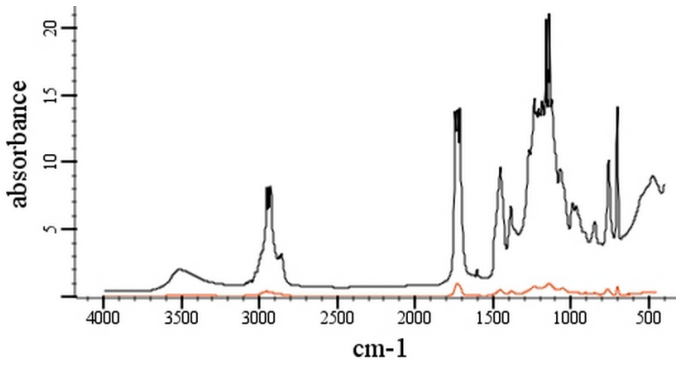

Figure 13: Peaks from the polymer coating sample (red) match those of acrylic resins, specifically Macrynal SM 510 (black).

4 Discussion

4.1 Visual Analysis

The uncustomary smooth surface and lack of corrosion at the rim flange area appears to indicate mechanical weathering in that region. This may have occurred during regular car use where the car pressed down and deformed the tire, causing the tire to rub against the metal at the flanges.

No clear filaments characteristic of filiform corrosion were observed; however, observation of these filaments was reported by the user at an earlier date. This may be due in part to evidence degradation- the tire-wheel assemblies were taken out of use in 2008 and left outdoors in the New England climate until 2010.

4.2 Crevice Corrosion

The thick concentration of white corrosion product at the bead seat area, where the bead of the tire sat on the rim, suggests a crevice corrosion mechanism. If moisture collected in this region, a stagnant solution would have been formed. Since oxygen diffusion into this zone is physically limited, the difference in oxygen concentrations would have caused the solution inside the crevice to act like an anode ($Al \rightarrow Al^{3+} + 3e^-$), and the exterior region to act like a cathode ($O_2 + 2H_2O + 4e^- \rightarrow 4OH^-$) [12-13]. The accumulation of Al^{3+} ions would encourage the influx of Cl^- ions resulting in the reaction:

$$AlCl_3 + 3H_2O \rightarrow Al(OH)_3 + 3H^+ + 3Cl^-$$

The high concentration of protons means that the solution inside the crevice would be acidic. Since Al^{3+} ions are used in this reaction, the tight contact between the rim and tire bead could have been compromised when the Al^{3+} ions went into solution. This situation could have been further exacerbated by the formation of $Al(OH)_3$. The addition of hydroxides to Al changes the FCC crystal structure of aluminum. The increased volume of the crystal could have weakened the intermolecular forces between the aluminum atoms, making them more likely to react with other compounds, thus accelerating the corrosive process.

4.3 Intergranular Corrosion

Aluminum is known to form a thin, oxidative film on its surface which normally protects it from corrosion. In order for intergranular attack to occur, the corrosion solution must penetrate through this layer, or the layer must not be present. It is possible that there was no protective oxide layer in this case because the alloy was polymer coated. In this case, the filiform corrosion which caused the plastic coating to flake off could have exposed the surface of the alloy to an unfavorable environment, which would have allowed corrosion to occur. Exposing the alloy to some combination of road salt or abrasive cleaning chemicals and water because it no longer had a coating could have caused the intergranular corrosion observed.

4.4 Protective Coatings

The filamentous corrosion that formed at the metal-lacquer interface is characteristic of filiform corrosion. Filiform corrosion is capable of forming filaments at a rate of 0.1 mm/day which produce white, gelatinous corrosion products that deform the lacquer layer [10, 13-14].

Filiform corrosion occurs because of contamination on or poor preparation of the surfaces being coated. The nature of the metal substrate's surface is critical to proper adhesion between the substrate and the protective coating [15]. Aside from the presence of filiform corrosion, the detachment of the lacquer in the form of flakes, instead of chips, indicates that the lack of adhesion appears to be the most likely cause of failure of the coating [16].

Failure to adhere may be the result of several factors. Proper adhesion requires a rough and clean surface [17]. Pre-treatment is usually accomplished by:

(1) Degreasing through the use of organic solvents, alkaline cleaning agents, or high-pressure steam with small concentrations of a cleaning agent.
(2) The roughening the surface of the metal- which is evident as small ridges on the rim [17],
(3) Blast cleaning by centrifugal or compressed air blasting with either dry or a sand-water mixture blown against the metal at high pressure [17].

If the rim cleaning process was not thorough enough, any presence of highly electronegative atoms, such as Cl, would bond preferentially to Al^{3+}, disrupting the natural passive film that protects aluminum from corrosion.

Defects could also result from the age of the lacquer that was applied. When lacquer is first applied, it must spread in order to cover the substrate. The viscosity of the liquid, which affects how well it spreads to cover the substrate, is affected by the amount of solvent present. The more solvent there is, the less viscous the liquid. However, in recent years, regulations have required lowering the amounts of volatile organic compounds (VOCs) used in paints. These VOCs are found in solvents. As a result, many industrial coatings have high initial viscosities that only increase upon mixing. These high viscosities can prevent lacquers from spreading properly, resulting in adhesion failure [15].

5 Conclusion

Several factors contributed to rapid deflation of the tire:

1. The poor adhesion of the acrylic coating led to filiform corrosion, which caused delamination of the protective film across much of the wheel rim and exposed the alloy to the outdoor environment;
2. The wheel geometry led to crevice corrosion; and
3. The aluminum alloy material was highly susceptible to intergranular corrosion due to the casting process.

Corroded rims on this specific wheel were a widespread problem, and that problem originated with the faulty acrylic coating. As such, the users of this wheel had no responsibility for the failure. Volkswagen sold the car, however, and should have taken responsibility for its actions. Replacing rims on a case-by-case basis was only a grudging way to admit it had sold a faulty product. Under these circumstances, Volkswagen is to blame and should have replaced corroded rims to ensure the safety and satisfaction of its customers.

6 Acknowledgements

Thanks go to Matt Neal for his excellent help using the lab equipment and to Jon Stolk for providing the opportunity to conduct this investigation and his guidance during the course of the investigation.

References

1. ProCarcare. *Cross-section*. 2009 [cited 2010 Dec. 10]; Available from: http://www.procarcare.com/images/shar/encyclopedia/8852NG04.gif.
2. Helsey, K. *Tire*. 2010 [cited 2010 Dec. 10]; Available from: http://www.khulsey.com/tire.jpeg.
3. Brookshier, K., Chin, E., Fox, R. 2010.
4. Pooz. *Information on Your Pitting Wheels Here*. 2003 13 Dec. 2003. [cited 2010 Nov 19]; Available from: http://forums.vwvortex.com/showthread.php?998602.
5. *Jetta Wolfsburg BBS Wheels*. May 2009 [cited 2010 Nov 19]; Available from: http://forums.generationdub.com/showthread.php?t=28510&page=1.
6. Reed, J. *How Do Rims & Wheels Differ?* 2010 [cited 2010 Nov 19]; Available from: http://www.ehow.com/how-does_4569434_rims-wheels-differ.html.
7. *Air Pressure- Correct, Underinflated and Overinflated*. Tire Tech Information/Air Pressure - Tire Inflation [cited 2010 Nov 19]; Available from: http://www.tirerack.com/tires/tiretech/techpage.jsp?techid=1.
8. Committee, A.S.M.I.H. and Knovel. *ASM handbook. Volume 15, Casting*. 2008.
9. Isakov, E., *Cast Contents*, in *Cutting Tool Engineering*. 2008.
10. Roberge, P.R., *Handbook of Corrosion Engineering*. 2000, McGraw-Hill.
11. *Product Guide - Liquid Coating Resins and Additives*. 2009 [cited 2010 Nov. 17]; Available from: http://www.cytec.com/liquids/Downloads/Liquid%20Coatings%20Resins%20and%20Additives-Product%20Guide_EMEA_En.pdf.
12. Shreir, L.L., R.A. Jarman, and G.T. Burstein, *Corrosion (3rd Edition) Volumes 1-2*. 1994, Elsevier.
13. Vargel, C., *Corrosion of Aluminium*. 2004, Elsevier.
14. Committee, A.S.M.I.H. and Knovel. *ASM handbook. Volume 13A, Corrosion: fundamentals, testing, and protection*. 2003.
15. Weldon, D.G., *Failure Analysis of Paints and Coatings*. 2002, John Wiley & Sons.
16. Mittal, K.L., *Adhesion Measurement of Films and Coatings, Volume 1*. 1995, VSP - An imprint of BRILL.
17. Bardal, E., *Corrosion and Protection*. 1st ed. 2003, New York: Springer.

Appendix

Calculations were as follows:

Based on the micrograph in Figure 8, an estimation of a 55% aluminum dendrite microstructure was made.

Referencing Figure 14, the lever rule was then used to estimate the initial aluminum weight percent based on this hypoeutectic structure.

□□□□□□□□ □□□□/□= □□□□□□/□□ □□□□□□□/□□ □+□

.55= 12.6−□□□□□□□ □□□□□/□ □□□□□□□□ □□□□□□□□12.6−1.6

□□□□□□□ □□□□□/□ □□□□□□□□ □□□□□□□□=*6.55%*

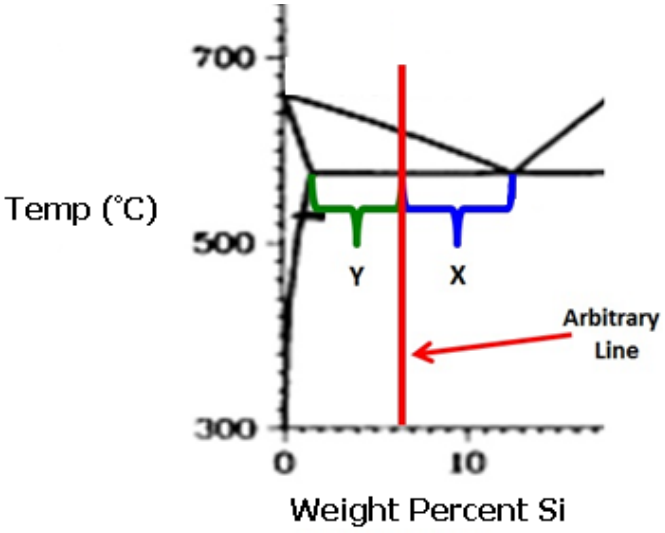

Figure 14: The aluminum-silicon phase diagram, modified to show calculations.